# SELECTIVE LASER SINTERING OF 13-93 BIOACTIVE GLASS

Krishna C. R. Kolan[1], Ming C. Leu[1], Gregory E. Hilmas[2] and Mariano Velez[3]
[1]Department of Mechanical and Aerospace Engineering, Missouri University of Science and Technology, Rolla, MO 65409
[2]Department of Materials Science and Engineering, Missouri University of Science and Technology, Rolla, MO 65409
[3]Mo-Sci Corporation, Rolla, MO 65401

## Abstract

Bioactive glasses are more promising than biopolymers in fabricating scaffolds for bone tissue repair because they convert to hydroxyapatite, when implanted *in vivo*. Both direct and indirect selective laser sintering (SLS) methods of 13-93 bioactive glass were considered in this research to study the feasibility of fabricating scaffolds for bone repair applications. Stearic acid was used as the binder in the indirect method to fabricate the scaffolds. The green scaffolds underwent binder burnout and sintering at various soaking conditions between $675^0C$ and $700^0C$, achieving a maximum compressive strength of 23.6 MPa, which is higher than that of the human cancellous bone. The sintered scaffolds had a pore size varying between 300 µm and 800 µm with 50% apparent porosity.

## 1. Introduction

The commonly used materials in fabrication of scaffolds for bone repair include metals and polymers. One of the major disadvantages of using these materials lies in the inability of the scaffolds to bond to a healthy bone. Several biopolymers such as poly-L-lactide (PLLA), Polycaprolactone (PCL), Polyetheretherketone (PEEK), etc. have been used to fabricate scaffolds [1-3]. In some cases, the biopolymers are mixed with Hydroxyapatite (HA), the main mineral constituent of bone, in different proportions to make the scaffold bioactive [4, 5]. The discovery of Bioglass by Hench led to the development of several other bioactive glasses with a similar composition [6]. 13-93 glass is a silicate based bioactive glass with a higher $SiO_2$ content, providing a better viscous flow than 45S5 glass, and could aid in porous scaffold fabrication [7]. The 13-93 glass showed promising results in terms of bioactivity in previous research [8, 9].

All the materials mentioned above, including 13-93 glass, have been used in fabricating scaffolds using traditional techniques such as solvent casting, freeze drying, foam replication, etc. The main drawback of using such techniques is the inability to fabricate a scaffold with the shape of a specific defect site and a controlled porous architecture. Freeform fabrication techniques, which can manufacture parts of complex shapes, can be used to overcome this limitation. Several additive manufacturing techniques like Stereolithography (SLA) [10], extrusion based techniques [11-13], 3D printing [14] and SLS [5, 15] have been used to fabricate scaffolds based on biopolymers, composite blends of biopolymer/HA and recently bioactive glasses. SLS of bioactive glass-ceramics was previously researched by Lorrison et. al. [16] and Goodridge et. al. [17], which demonstrated the potential of this process in fabrication of scaffolds using bioactive glasses.

In the current work, we investigate the feasibility of using 13-93 glass to fabricate scaffolds for bone repair applications using both direct and indirect SLS methods. This paper explains the materials used and methods of analysis, followed by a section explaining the direct

and indirect sintering of 13-93 glass. The effects of key parameters on fabrication of cylindrical scaffolds are discussed. The results obtained including the compressive strengths are presented.

## 2. Materials and Methods

### 2.1. Preparation of powder

13-93 bioactive glass (prepared by Mo-Sci Corp. code: GL-0811) with a nominal chemical composition of 53% $SiO_2$, 4% $P_2O_5$, 20% CaO, 5% MgO, 6% $Na_2O$ and 12% $K_2O$ (in weight %) was made from high-purity chemical reagents by melting several batches of raw materials in 5-kg capacity platinum crucibles and quenching the molten material of glass in water. The chemical composition of the quenched glass was confirmed by XRF (X-ray fluorescence analysis). The quenched glass was milled and sieved to a particle size below 75 µm. The milled 13-93 glass was mixed in a V-blender with stearic acid ($C_{18}H_{36}O_2$, grade HS, Acros Organics) and dry ball-milled for 8 hours with $ZrO_2$ grinding medium to obtain powders with mixing ratios of 50:50 and 60:40 (13-93 glass to stearic acid) in volume %.

### 2.2. Selective laser sintering

All the fabrication experiments were carried out on a commercial DTM Sinterstation 2000 machine. A detail description of the machine and its parameters is available from literature [18, 19]. Both direct and indirect SLS methods were employed in this study to establish a feasible set of SLS parameters conducive to fabricate scaffolds using 13-93 glass. In the direct method, bare 13-93 glass powder is used as the feedstock to the SLS machine. In the indirect method, stearic acid is mixed with the 13-93 glass powder to help fuse the powder particles during fabrication. An initial set of experiments were conducted using both methods to understand the behavior of the materials under the scanning of laser beam. In the direct method, mono layers were fabricated at different laser power, scan speed and scan spacing to study the effects of these parameters. The part bed temperature and part heater temperature should have been maintained near the glass transition temperature ($T_g$) of 13-93 glass, which is around $600^o$C, to ease the laser sintering. However, these parameters were not considered in the direct method as the DTM 2000 Sinterstation was technically not capable of reaching near the $T_g$. In the indirect method, both the part bed and part heater temperatures have been maintained just below the melting point of binder, which aids in binder melting with low laser power and avoids unnecessary buildup of heat in the part bed [20]. A post-processing step is involved in the indirect method to burn out the binder and then sinter the 13-93 glass particles.

### 2.3. Post-processing and Analysis

All the powders (13-93 glass, stearic acid and 13-93/stearic acid at 50:50 and 60:40 ratios by volume) used for fabrication were examined by differential scanning calorimetry (DSC) (TA Instruments, SDT Q600, Utah) and differential thermal analysis (DTA) (NETZSCH simultaneous DTA/TGA). All the green parts were post-processed in a three stage programmable air furnace (Vulcan Benchtop Furnace, York, PA). SEM (Hitachi S-570, Japan) images of the sintered parts were obtained to analyze the microstructures. Mechanical testing was performed on the sintered scaffolds to determine their compressive strength using a mechanical load frame (Instron 4469 UTM, Norwood, MA) at a cross-head speed of 0.5 mm/min. The amorphous nature of both the mono layer fabricated using the direct SLS method and post-processed scaffolds fabricated using the indirect SLS method, was confirmed by running a powder X-ray

diffraction (XRD) analysis (Philips X-Pert, Westborough, MA) using Cu Kα radiation (λ = 0.154056 nm). Scans were run from 2θ values ranging from $10^o$ to $80^o$.

## 3. Fabrication

### 3.1. Direct selective laser sintering

As mentioned in Section 2.2, the effects of SLS process parameters were studied by fabricating mono layers in this method. The laser power was varied from 5W to 50W, scan speed from 50.8 mm/s to 406.4 mm/s, and different scan spacings and energy densities were explored. The scan speed and scan spacing were varied from the minimum possible of the SLS machine to attain higher energy densities. Energy density is an important parameter which relates the three process parameters of scan speed, scan spacing and laser power as below [21]:

$$\text{Energy Density} = \text{Laser Power} / (\text{Scan Speed x Scan Spacing}) \dots\dots\dots\dots\dots\dots (1)$$

During the initial set of experiments, it was observed that the 13-93 glass started to soften and form "balls" at 20W laser power, 127 mm/s scan speed and at 0.228 mm scan spacing. The 13-93 glass requires higher energy density, which could be obtained only by reducing the scan speed and scan spacing to the minimum. By varying one parameter and maintaining the other two parameters constant, the effect of each parameter is studied and the best results were observed at 50.8 mm/s scan speed and 0.076 mm scan spacing (both values are minimum available for the machine). Figure 1 shows the effects of parameters on the mono layers, where Figure 1(a) shows the effect of scan speed and Figure 1(b) shows the effect of scan spacing while maintaining the laser power at 25W. In both cases, consistent with the observations previously reported by other researchers [22-26], "balling effect" was observed at lower energy densities. It has also been observed that an increase in energy density increased the "ball" diameter. This is also consistent with the results reported by Klocke and Wagner [24] in their line scanning experiments. However, with a low scan speed and scan spacing (minimum possible in our case), but at lower laser power, which reduce the energy densities relatively, the "balling effect" was reduced. One such mono layer, which was sintered at 20W laser power, 50.8 mm/s scan speed and 0.076 mm scan spacing, is shown in Figure 2. Further reduction in the laser power affects the "balling effect", which can be clearly seen in Figure 1(c). As the laser beam scans at a slow speed with reduced scan spacing, the "balls" sinter together to form surface bands in the direction of the beam scanning. The formation of surface bands during the direct selective laser sintering process was previously studied by Fan et. al. [27] and Song et. al. [28]. Agarwala et. al. [25] reduced the "balling effect" in their work by increasing the part bed temperature, which is difficult in our case as explained in Section 2.2. Fabrication issues in direct SLS of ceramics are not explored by researchers nearly as much when compared to direct SLS of metals. Direct SLS of bioactive glass-ceramics was previously investigated by Lorrison et. al. [16]. The results showed a similar surface grooves or bands, to a lesser extent, on the direct SLS part fabricated by them using an experimental SLS machine, which has low scan speeds and higher powers compared to the commercial SLS machine used in our research work. In our current study, because of the highly porous nature in the mono layer when directly sintered, fabrication of 3D part was difficult because of difficulties in spreading the powder and bonding between the successive layers. The current research did not include the effect of particle size, which will have its effect in the fabrication process as a smaller particle size would require less heat to melt [28]. Further

reduction in scan speed, scan spacing (using an advanced SLS machine) and particle size combined with effective packing of powder particles in the part bed could give better results in the direct SLS of 13-93 glass. This needs to be further explored in the future.
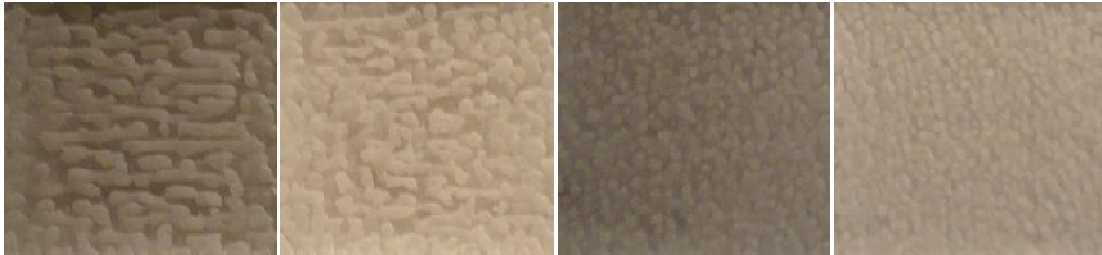


(a) Effect of Scan speed (L-R: 50.8, 76.2, 101.6 and 127 mm/s) at Laser power = 25W and Scan spacing = 0.076 mm



(b) Effect of Scan spacing (L-R: 0.076, 0.101, 0.127 and 0.152 mm) at Laser power = 25W and Scan speed = 50.8 mm/s



(c) Effect of Laser power (L-R: 15, 20, 22 and 25 W) at Scan speed = 50.8 mm/s and Scan spacing = 0.076 mm

Figure 1. Effects of scan speed, scan spacing and laser power



Figure 2. Mono layer laser sintered at 20W (25.4 mm x 25.4 mm)

## 3.2. Indirect selective laser sintering

In the indirect SLS method, a polymeric binder, stearic acid (SA), was used to mix with the 13-93 glass powder. SA was successfully used as a binder in our previous study to produce zirconium diboride components [18]. The SA flakes got crushed to very fine particles after ball milling and adhered to the surface of 13-93 glass particles. SA left little or no carbon residue during the burnout stage in the current study. The energy provided by the laser melted the stearic acid, which fused the 13-93 glass particles together to form a green part. Green parts were successfully fabricated using powder compositions in two different proportions, i.e., 40% and 50% binder content by volume.

An experimental approach was used to determine the feasible set of parameters in fabricating the green parts. An experiment was conducted to check the degree of melting of SA by varying the energy density from 0.84 cal/cm$^2$ to 2.74 cal/cm$^2$. By means of visual inspection, an energy density of 1 cal/cm$^2$ was determined to be sufficient enough to melt the SA. Several parts measuring 25.4 mm x 25.4 mm and 1mm thick were fabricated at laser powers of 2W and 3W and with varying scan speeds, thereby maintaining energy density at 1 cal/cm$^2$, to study the bonding between successive layers. The best bonding was achieved with 3W laser power, 304.8 mm/s scan speed, and 0.229 mm scan spacing. The part bed and part heater temperatures were maintained at 60$^o$C, just below the melting point of SA.

Figure 3 shows the CAD model of a cylindrical porous scaffold with a designed porosity of 58.8%, pore width of 1 mm, and wall thickness of 1 mm. Figure 4 shows the green parts fabricated using these process parameters. Figure 4(a) shows the green part fabricated with 50 vol % SA and layer thickness of 0.152 mm. As the binder content is reduced, less amount of binder content is available to fuse the 13-93 glass particles not only to fuse the current layer but also to fuse the layer below, which causes delamination. To reduce the delamination, the layer thickness was reduced to 0.1 mm. Figure 4(b) shows the green part fabricated with 40 vol % SA and layer thickness of 0.1 mm. The part fabricated with 40 vol % SA had higher green strength. Further reduction of binder content would require reducing the layer thickness to 0.076 mm (min available for Sinterstation 2000). This was not considered because of the 13-93 glass particle size used in this study (in the range of <75 μm), which would have caused difficulties in spreading the powder. Smaller layer thickness can be used with smaller particle size, which could reduce the binder content. The effect of particle size and optimizing the binder content will be investigated in our future work.
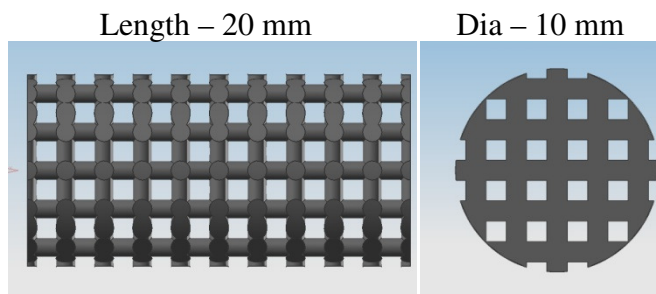


Length – 20 mm    Dia – 10 mm
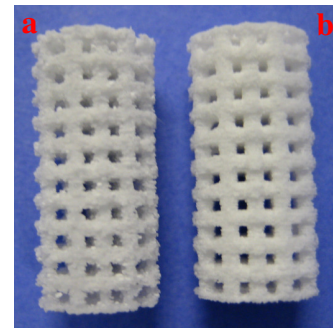
Figure 3. CAD model of the porous scaffold



Figure 4. Green parts

# 4. Results

After the fabrication of the green parts, a heat treatment schedule was developed based on the DSC-TGA curve of stearic acid. The binder burnout and sintering was carried out in a three stage programmable bench-top air furnace. All the samples were sintered at temperatures ranging from $675^{\circ}C$ to $700^{\circ}C$. The scaffolds fabricated using 50 vol % SA and sintered at $675^{\circ}C$ for 1 hr had low compressive strengths, ranging 5 – 11 MPa. Hence, the scaffolds fabricated using 40 vol % SA were sintered at $685^{\circ}C$ and $695^{\circ}C$ with two different hold times. The maximum shrinkage was observed for the scaffold sintered at $695^{\circ}C$ for 1 hr, and was around 22.6 % length wise. The shrinkage values listed in Table 1 are length-wise when compared to green part. The apparent porosities of scaffolds were measured following the ASTM C373 standard method. The compressive tests on scaffolds show an increase in the strength with increasing the sintering temperature and duration. A maximum compressive strength of 23.6 MPa was measured for a scaffold sintered at $695^{\circ}C$ for 1 hr, which is higher than the trabecular bone. Table 1 shows the average compressive strengths of the scaffolds evaluated. The pore size varied from 300 μm to 800 μm, which could result in better bone growth than having pore size less than 100 μm [29, 30].

Table 1. Effect of soaking conditions on properties of 60:40 13-93/SA scaffolds

| Soaking conditions | Shrinkage (%) | Porosity (%) | Compressive strength (MPa) |
|---|---|---|---|
| $685^{\circ}C$ - 0.5 hr | 20.0 | 53.2 | 12.2 ± 2.4 |
| $685^{\circ}C$ - 1 hr | 21.7 | 50.7 | 13.2 ± 2.4 |
| $695^{\circ}C$ - 0.5 hr | 20.5 | 53.5 | 15.3 ± 4.9 |
| $695^{\circ}C$ - 1 hr | 22.6 | 50.3 | 20.4 ± 2.2 |

Figure 5 shows the XRD patterns of the as-received 13-93 glass, processed 13-93 glass using direct SLS and indirect SLS methods. It can be clearly seen that the 13-93 glass maintained its amorphous nature when processed using both methods. The crystallization of bioactive glasses prior to implantation could slow down the mineralization process [7].
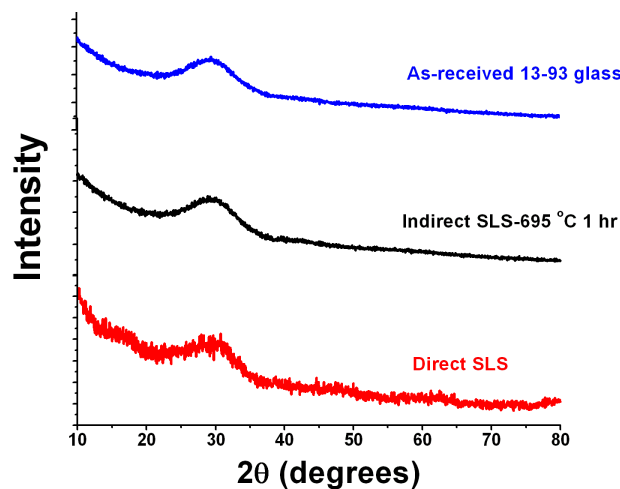


Figure 5. XRD patterns of the 13-93 glass

Figure 6 shows a scaffold sintered at 695°C for 1 hr and Figure 7 shows the SEM image of a fractured surface of the sintered scaffold. The SEM image shows a rough surface, which could be conducive for better cell growth. The voids in the walls are formed because of the higher amount of binder used in the fabrication. The presence of voids decreases the compressive strength of the scaffold. Reducing the size of voids in the walls of the scaffold by optimizing the binder content and heat treatment schedule will be considered in our future work. Binder burnout is one of the critical stages during the heat treatment schedule in the indirect SLS method, especially while fabricating scaffolds with interconnected pores and controlled porosity, because the porous scaffold should maintain its structural integrity.
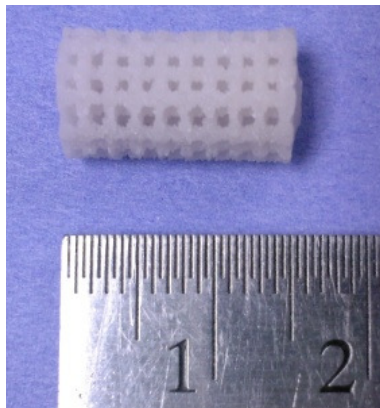


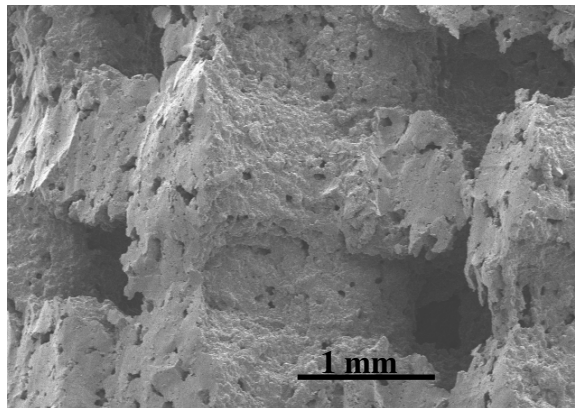Figure 6. Scaffold sintered at 695°C for 1 hr



Figure 7. SEM image of fractured surface

## 5. Conclusion

The main research objective of this work was to study the feasibility of fabricating a scaffold for bone repair applications with 13-93 bioactive glass using both direct and indirect SLS methods. The obtained results from direct SLS exposed the limitations in 3D part fabrication with direct laser sintering of the 13-93 glass. The future prospect lies on the ability of 13-93 glass to maintain its amorphous nature even after being directly processed by the laser. With future advances in SLS machines and optimal selection of process parameters and particle size, it may be possible to fabricate a 3D structure by direct SLS.

The obtained results from indirect SLS method have demonstrated successful use of this technique to fabricate 13-93 glass scaffolds for bone tissue engineering. The average compressive strength of the fabricated scaffolds after post-processing was 20.4 MPa, which is the highest ever reported for a bioactive glass scaffold with controlled porosity fabricated using the SLS process. Also, the strengths reported are higher than those of the trabecular bone. This demonstrates the high potential of using 13-93 bioactive glass scaffolds for replacement of human trabecular bones, by designing and fabricating scaffolds with similar internal architectures.

**References**

[1]    R. Y. Zhang and P. X. Ma, "Porous poly(L-lactic acid)/apatite composites created by biomimetic process," *Biomed Mater Res.,* 45 (4), 285–293, (1999).

[2]    D. W. Hutmacher, T. Schantz, I. Zein, K. W. Ng, S. H. Teoh and K. C. Tan, "Mechanical properties and cell cultural response of polycaprolactone scaffolds designed and fabricated via fused deposition modeling," *J. Biomed Mater Res A*, 55 [2] 203-216 (2001).

[3]    K. H. Tan, C. K. Chua, K. F. Leong, C. M. Cheah, W. S. Gui and W. S. Tan *et al.*, "Selective laser sintering of biocompatible polymers for applications in tissue engineering," *Bio-med Mater Eng UK,* 15 (1–2), 113–124, (2005).

[4]    F. E. Wiria, K. F. Leong, C. K. Chua and Y. Liu, "Poly-e-caprolactone/hydroxyapatite for tissue engineering scaffolds fabrication via selective laser sintering," *Acta Biomater,* 3 (1), 1–12 (2007).

[5]    F. E. Wiria, C. K. Chua, K. F. Leong, Z. Y. Quah, M. Chandrasekaran and M. W. Lee, "Improved biocomposite development of poly(vinyl alcohol) and hydroxyapatite for tissue engineering scaffold fabrication using selective laser sintering," *J Mater Sci Mater Med.,* 19 (3), 989–996 (2008).

[6]    L.L. Hench, "The story of bioglass," *J. Mater. Sci. Mater. Med.,* 17 (11), 967–978, (2006).

[7]    M. N. Rahaman, R. F. Brown, B. S. Bal, and D. E. Day, "Bioactive Glasses for Nonbearing Applications in Total Joint Replacement," *Semin. Arthroplasty*, 17, 102–12 (2006).

[8]    R. F. Brown, D. E. Day, T. E. Day, S. Jung, M. N. Rahaman and Q. Fu, "Growth and differentiation of osteoblastic cells on 13–93 bioactive glass fibers and scaffolds," *Acta Biomaterialia,* 4, 387–396, (2008).

[9]    Q. Fu, M. N. Rahaman, W. Huang, D. E. Day and B. S. Bal, "Preparation and bioactive characteristics of a porous 13-93 glass, and its fabrication into the articulating surface of a proximal tibia," *J. Biomed. Mater. Res.,* 82A, 222-9, (2007).

[10]   T. Matsuda and T. Mizutani, "Liquid Acrylate-endcapped Biodegrable Poly(e-caprolactone-co-trimethylene Carbonate) II Computer-aided sterolithographic microarchitectural surface photoconstructs," *J. Biomed. Mater. Res.,* 62, 395-403, (2002).

[11]   F. C. Gomes de Sousa and J. R. Evans, "Sintered Hydroxyapatite Latticework for Bone Substitute," *J. Am. Ceram. Soc.*, 86 [3], 517-519, (2003).

[12]   J. Cesarano III, J. G. Dellinger, M. P. Saavedra, and D. D. Gill, "Customization of Load-Bearing Hydroxyapatite Lattice Scaffolds," *Int. J. Appl. Ceram. Technol.*, 2 [3] 212–220, (2005).

[13]   S. Hsu, H. Yen, C. Tseng, C. Cheng, and C. Tsai, "Evaluation of the growth of chondrocytes and osteoblasts seeded into precision scaffolds fabricated by fused deposition manufacturing," *J Biomed Mater Res B Appl Biomater.*, 80B [2] 519-527 (2006).

[14]   A. Rainer, S. M. Giannitelli, F. Abbruzzese, E. Traversa, S. Licoccia and M. Trombetta, "Fabrication of bioactive glass–ceramic foams mimicking human bone portions for regenerative medicine," *Acta Biomaterialia*, 4 [2], 362-369, (2008).

[15]   J. M. Williams and S. Das, "Bone tissue engineering using polycaprolactone scaffolds fabricated via selective laser sintering," *Biomaterials,* 26, 4817 – 4827, (2005).

[16] J. C. Lorrison, R. D. Goodridge, K. W. Dalgarno, and D. J. Wood, "Selective Laser Sintering of Bioactive Glass-Ceramics," Solid Freeform Fabrication Proceedings, Austin, Texas, 1-8 (2002).

[17] R. D. Goodridge, K. W. Dalgarno, and D. J. Wood, "Indirect selective laser sintering of an apatite–mullite glass-ceramic for potential use in bone replacement applications," *J. Engineering in Med H*, 220, (2006).

[18] M. C. Leu, E. B. Adamek, T. Huang, G. E. Hilmas and F. Dogan, "Freeform Fabrication of Zirconium Diboride Parts Using Selective Laser Sintering," Proceedings of Solid Freeform Fabrication Symposium, Austin, Texas, August 4-6, (2008).

[19] S. Pattnaik, "Investigation of zirconium diboride parts using selective laser sintering," Thesis (MS), Missouri University of Science and Technology, Rolla, (2009).

[20] I. Gibson and D. Shi, "Material properties and fabrication parameters in selective laser sintering process," *Rapid Prototyping Journal*, 3 (4), 129-136, (1997).

[21] J. C. Nelson, "Selective Laser Sintering: A definition of the process and an empirical sintering model," Dissertation (PhD), University of Texas, Austin, (1993).

[22] F. Abe, K. Osakada, M. Shiomi, K. Uematsu and M. Matsumoto, "The manufacturing of hard tools from metallic powders by selective laser melting," *J. Materials Processing Technology,* 111 (1–3), 210–213, (2001).

[23] C. Hauser, T. H. C. Childs, K. W. Dalgarno and R. B. Eane, "Atmospheric control during direct selective laser sintering of stainless steel 314s powder," Proceedings of Solid Freeform Fabrication Symposium, Austin, Texas, 265–272, (1999).

[24] F. Klocke and C. Wagner, "Coalescence behavior of two metallic particles as base mechanism of selective laser sintering," *CIRP Annals* 52 (1), 177–184, (2003).

[25] M. K. Agarwala, D. L. Bourell, J. Beaman, H. Marcus and J. Barlow, "Direct selective laser sintering of metals," *Rapid Prototyping Journal*, 1 (1), 26–36 (1995).

[26] T. H. C. Childs, C. Hauser and M. Badrossamay, "Selective laser sintering (melting) of stainless and tool steel powders: experiments and modeling," *Proc. IMechE part B, J. Engineering Manufacture,* 219, 339–357, (2005).

[27] K. M. Fan, W. L. Cheung and I. Gibson, "Movement of powder bed material during the selective laser sintering of bisphenol A polycarbonate," *Rapid Prototyping Journal*, 11 (4), (2005).

[28] Y. A. Song, "Experimental study of the basic process mechanism for direct selective laser sintering of low-melting metallic powder," *Ann. CIRP, Manufacturing Technol.* 46, 127–130, (1997).

[29] C. M. Murphy, M. G. Haugh and F. J. O'Brien, "The effect of mean pore size on cell attachment, proliferation and migration in collagen–glycosaminoglycan scaffolds for bone tissue engineering," *Biomaterials*, 31, [3], 461-466, (2010).

[30] V. Karageorgiou and D. Kaplan, "Review: Porosity of 3D biomaterial scaffolds and osteogenesis," *Biomaterials*, 26, [27], 5474-5491, (2005).